

The noise propagator in an optical system using EDFAs and its effect on system performance: accurate evaluation based on linear perturbation

Zhongxi Zhang*, Liang Chen, Xiaoyi Bao

Department of Physics, University of Ottawa, 150 Louis Pasteur, Ottawa, K1N 6N5, Canada

[*zzhan3@uottawa.ca](mailto:zzhan3@uottawa.ca)

Abstract: For optical systems amplified by EDFAs, we present a new approach to obtain the noise propagator from the accurate linearized noise equation (LNE) proposed by Holzlohner *et al* [1]. With the help of fourth-order Runge-Kutta in the interaction picture (RK4IP) method, we solve both the accurate LNE and the nonlinear Schrödinger equation (NLSE) for the noise-free signal simultaneously. The noise propagator matrix thus obtained does not need the jitter separation required by the covariance matrix method (CMM) [1]. Based on this new approach, the calculated BER in a DPSK system agrees well with the simulation using CMM. By introducing a deterministic phase shift induced by Gordon-Mollenauer noise effect, our numerical results also agree well with the experimental data of multi-span DPSK systems.

© 2012 Optical Society of America

OCIS codes: (060.2330) Fiber optics communications; (060.4370) Nonlinear optics, fiber; (060.5060) Phase modulation; (190.4410) Nonlinear optics, parametric process.

References and links

1. R. Holzlohner, V. S. Grigoryan, C. R. Menyuk, and W. L. Kath, "Accurate calculation of eye diagrams and bit error rates in optical transmission systems using linearization," *J. Lightwave Technol.* **20**, 389-400 (2002).
2. K. Kikuchi, "Enhancement of optical-amplifier noise by nonlinear refractive index and group-velocity dispersion of optical fibers," *IEEE Photon. Technol. Lett.* **5**, 1079-1081 (1993).
3. A. Carena, V. Curri, R. Gaudino, P. Poggiolini, and S. Benedetto, "New analytical results on fiber parametric gain and its effects on ASE noise," *IEEE Photon. Technol. Lett.* **9**, 535-537 (1997).
4. R. Hui, M. O'Sullivan, A. Robinson, and M. Taylor, "Modulation instability and its impact in multispan optical amplified IMDD systems: theory and experiments," *J. Lightwave Technol.* **15**, 1071-1082 (1997).
5. P. Serena, A. Orlandini, and A. Bononi, "Parametric-gain approach to the analysis of single-channel DPSK/DQPSK systems with nonlinear phase noise," *J. Lightwave Technol.* **24**, 2026-2037 (2006).
6. A. Demir, "Nonlinear phase noise in optical-fiber-communication systems," *J. Lightwave Technol.* **25**, 2002-2032 (2007).
7. L. D. Coelho, L. Molle, D. Gross, N. Hanik, R. Freund, C. Caspar, E.-D. Schmidt, and B. Spinnler, "Modeling nonlinear phase noise in differentially phase-modulated optical communication systems," *Opt. Express* **17**, 3226-3241 (2009).
8. M. Secondini, E. Forestieri, C. R. Menyuk, "A combined regular-logarithmic perturbation method for signal-noise interaction in amplified optical systems," *J. Lightwave Technol.* **27**, 3358-3369 (2009).
9. R. Holzlohner, C. R. Menyuk and W. L. Kath, "Efficient and accurate computation of eye diagrams and bit error rates in a single-channel CRZ system," *IEEE Photon. Technol. Lett.* **14**, 1079-1081 (2002).
10. R. Holzlohner, C. R. Menyuk and W. L. Kath, "A covariance matrix method to compute bit error rates in a highly nonlinear dispersion-managed soliton system," *IEEE Photon. Technol. Lett.* **15**, 688-690 (2003).

11. R. Holzlohner and C. R. Menyuk, "Use of multicanonical Monte Carlo simulations to obtain accurate bit error rates in optical communications systems," *Opt. Lett.* **28**, 1894-1896 (2003).
12. A. Demir, "Non-Monte Carlo formulations and computational techniques for the stochastic nonlinear Schrödinger equation," *J. Comput. Phys.* **201**, 148-171 (2004).
13. J. Hult, "A fourth-order Runge-Kutta in the interaction picture method for simulating supercontinuum generation in optical fibers," *J. Lightwave Technol.* **25**, 3770-3775 (2007).
14. Z. Zhang, L. Chen, and X. Bao, "A fourth-order Runge-Kutta in the interaction picture method for numerically solving the coupled nonlinear Schrödinger equation," *Opt. Express*, **18**, 8261-8276 (2010).
15. J. P. Gordon and L. F. Mollenauer, "Phase noise in photonic communications systems using linear amplifiers" *Opt. Lett.* **15**, 1351-1353 (1990).
16. A.M. Mathai and S.B. Provost, *Quadratic Forms in Random Variables: Theory and Applications*. Marcel Dekker, New York, (1992).
17. E. Forestieri, "Evaluating the error probability in lightwave systems with chromatic dispersion, arbitrary pulse shape and pre- and postdetection filtering," *J. Lightwave Technol.* **18**, 1493-1503 (2000).
18. Z. Zhang, L. Chen, and X. Bao, "Accurate BER evaluation for lumped DPSK and OOK systems with PMD and PDL," *Opt. Express*, **15**, 9418-9433, (2007).
19. D. Gariépy and G. He, "Measuring OSNR in WDM systems Effects of resolution bandwidth and optical rejection ratio" White paper, EXFO Inc. (2009).
20. P. Serena, A. Bononi, J.-C. Antona, and S. Bigo, "Parametric gain in the strongly nonlinear regime and its impact on 10-Gb/s NRZ systems with forward-error correction" *J. Lightwave Technol.* **23**, 2352-2363 (2006).
21. A. Bononi, P. Serena, and A. Orlandini, "A unified design framework for single-channel dispersion-managed terrestrial systems," *J. Lightwave Technol.* **26**, 3617-3631 (2008).
22. E. Ip and J. M. Kahn, "Power spectra of return-to-zero optical signals," *J. Lightwave Technol.* **24**, 1610-1618 (2006).
23. A. Papoulis, *Probability, Random Variables, Stochastic Processes*. New York: McGraw-Hill, 1991.
24. E. Forestieri and G. Prati, "Exact analytical evaluation of second-order PMD impact on the outage probability for a compensated system," *J. Lightwave Technol.* **22**, 988-996 (2004).

1. Introduction

The amplified spontaneous emission (ASE) noise generated from optical amplifiers, e.g., Erbium Doped Fiber Amplifiers (EDFAs), is one of the basic reasons for the bit-error-rate (BER) in an optical fiber communication (OFC) system. For an OFC system with non-negligible Kerr nonlinearity, the ASE impact evaluation is complicated because of the nonlinear interaction between signal and ASE noise. In the case of signal field being much stronger than the noise field, the noise-noise beating is relatively small so that the noise field in the fiber can be approximately described by an equation called linearized noise equation (LNE), which was proposed separately in Ref. [1] and Refs. [2]-[8].

Noise propagator is a matrix introduced to describe the noise propagation in the fiber. Within the framework of linear perturbation, it is independent of the specific noise realizations and can be used to evaluate the noise impact on the moment-generating function (MGF) of the filtered photoelectric current and then on the BER at the receiver [1, 5, 7, 8].

The popular form of LNE [2]-[8] is based on the continuous wave (CW) assumption, i.e., the noise-free signal in the LNE is artificially simplified as a CW wave. As a result, a semi-analytical form of noise propagator and the noise power spectral density (PSD), usually called parametric gain (PG), can be obtained. The drawback of this simplification is that the noise-free signal in this LNE has no chromatic dispersion (CD) effect. Thus the couplings between noise components (in frequency domain) cannot be taken into account.

A LNE beyond CW, named accurate LNE in this work, was first proposed and discussed in Ref. [1]. Dynamically taking into account the local CD and Kerr nonlinearity along the fiber, this LNE provides accurate noise information, with its computational cost being much higher than the CW approach. As an example, given a noise-free signal obtained from NLSE, the computation required to update the accurate LNE has cubic complexity in the number of Fourier components [1]. To reduce the computational complexity, covariance matrix method (CMM) was proposed in Ref. [1], where the noise covariance matrix was obtained by processing large

enough noise realizations. In Refs. [9, 10], the computational cost of CMM was further reduced by a deterministic approach using perturbation solution. Since the raw covariance matrix obtained either by noise realizations [1] or by deterministic approach [9, 10] may contain nonlinear noise contribution, it is important to separate the nonlinearity-induced phase jitter and, in some cases, time jitter from the raw covariance matrix. Thus, the obtained pdfs of the receiver voltage agrees well with Monte Carlo simulation [1, 9, 11].

Based on linear perturbation, the noise covariance matrix can also be obtained by solving its ordinary differential equation (ODE) proposed by [1, 12]. The covariance matrix obtained by solving such linear ODE does not need jitter separation, although this ODE is more complicated than the accurate LNE [12]. So far there is little comparison between the approaches of Ref. [12] and Refs. [1, 9, 10].

In this work, we show that the noise propagator matrix can be obtained directly from the accurate LNE. Therefore, there is no nonlinearity-induced jitter in such noise propagator. To effectively reduce the computational complexity in updating the LNE, one can decompose the Kerr effect related matrix into a symmetric and an antisymmetric matrices [cf. the discussion after Eq. (36) in the Appendix]. Also, to solve the accurate LNE with large enough step size, the fourth-order Runge-Kutta in the interaction picture (RK4IP) method [13, 14] is generalized and applied, as shown in Sec. 2. Based on Refs. [1, 5, 7, 8], we evaluate the impacts of noise propagator on MGF and BER in Sec. 3. The accuracy of this new approach depends on how far the linearized noise deviates from the actual noise. To numerically verify this new approach, we calculate the BERs in a 20-span DPSK system discussed in Ref. [5], where the CMM results with nonlinear phase noise $\Phi_N = 0.2\pi$ were given. Our BER calculations agree well with the CMM results. We also consider the experimental data of the multi-span DPSK systems in Ref. [7]. A new phase shift is introduced to fit the experimental data. This new deterministic shift is determined by the variance of the Gordon-Mollenauer (GM) phase noise [15].

2. Noise propagator obtained from the accurate LNE

Within the framework of linear perturbation, the noise propagator in an EDFA-based system is a fundamental matrix that determines the noise impacts on MGF and BER. In this section, we show that the noise propagator matrix in a fiber of length L can be obtained from the accurate LNE given by Eq. (38). For a multi-span OFC system, one needs to introduce an equivalent noise propagator which can be obtained by calculating the PG.

2.1. Noise propagator in a fiber of length L

The noise propagator in a fiber of length L can be obtained by extending the RK4IP in Refs. [13, 14] to the LNE (38). By introducing $\tilde{a} = e^{\hat{L}(z-z_0)} \tilde{a}^I$ and $\hat{N}^I = e^{-\hat{L}(z-z_0)} \hat{N} e^{\hat{L}(z-z_0)} = e^{-\hat{L}(z-z_0)} (\hat{v} + \hat{\mu}) e^{\hat{L}(z-z_0)}$, Eq. (38) in the interaction picture (IP) has the form

$$\frac{d\tilde{a}^I}{dz} = \hat{N}^I \tilde{a}^I \quad (1)$$

Taking $z_0 = z_n + h/2$ with $h = z_{n+1} - z_n$ and denoting $\tilde{a}_n = \tilde{a}(z_n)$, $\tilde{a}_{n+1} = \tilde{a}(z_{n+1})$, $\hat{N}_n^I = e^{\hat{N}h/2} \hat{N}(z_n) e^{-\hat{N}h/2}$, $\hat{N}_{n+1/2}^I = \hat{N}(z_n + h/2)$, and $\hat{N}_{n+1}^I = e^{-\hat{L}h/2} \hat{N}(z_{n+1}) e^{\hat{L}h/2}$, one can use RK4IP [13, 14] to solve Eq. (1) with

$$\begin{aligned} \tilde{a}_{n+1} &= e^{\hat{L}h/2} [\tilde{a}_n^I + \frac{hk_1}{6} + \frac{hk_2}{3} + \frac{hk_3}{3} + \frac{hk_4}{6}] \\ \tilde{a}_n^I &= e^{\hat{L}h/2} \tilde{a}_n \\ k_1 &= \hat{N}_n^I \tilde{a}_n^I = e^{\hat{L}h/2} \hat{N}(z_n) \tilde{a}_n \equiv \hat{k}_1 \tilde{a}_n \end{aligned}$$

$$\begin{aligned}
k_2 &= \hat{N}_{n+1/2}^I [\tilde{a}_n^I + \frac{hk_1}{2}] = \hat{N}(z_n + h/2) [e^{\hat{L}h/2} + \frac{h\hat{k}_1}{2}] \tilde{a}_n \equiv \hat{k}_2 \tilde{a}_n \\
k_3 &= \hat{N}_{n+1/2}^I [\tilde{a}_n^I + \frac{hk_2}{2}] = \hat{N}(z_n + h/2) [e^{\hat{L}h/2} + \frac{h\hat{k}_2}{2}] \tilde{a}_n \equiv \hat{k}_3 \tilde{a}_n \\
k_4 &= \hat{N}_{n+1}^I [\tilde{a}_n^I + hk_3] = e^{-\hat{L}h/2} \hat{N}(z_{n+1}) e^{\hat{L}h/2} [e^{\hat{L}h/2} + h\hat{k}_3] \tilde{a}_n \equiv \hat{k}_4 \tilde{a}_n
\end{aligned} \tag{2}$$

or

$$\tilde{a}_{n+1} = \left(e^{\hat{L}h/2} \left[e^{\hat{L}h/2} + \frac{h\hat{k}_1}{6} + \frac{h\hat{k}_2}{3} + \frac{h\hat{k}_3}{3} \right] + \frac{h}{6} \hat{N}(z_{n+1}) e^{\hat{L}h/2} (e^{\hat{L}h/2} + h\hat{k}_3) \right) \tilde{a}_n, \tag{3}$$

which means the noise propagator for the fiber of length $h = z_{n+1} - z_n$ can be calculated as

$$H(z_{n+1}, z_n) = e^{\hat{L}h/2} \left[e^{\hat{L}h/2} + \frac{1}{3} \left(\frac{h}{2} \hat{k}_1 + \frac{2h}{2} \hat{k}_2 + h\hat{k}_3 \right) \right] + \frac{h}{6} \hat{N}(z_{n+1}) e^{\hat{L}h/2} [e^{\hat{L}h/2} + h\hat{k}_3] \tag{4}$$

For the fiber of length L , the noise propagator has the form

$$p_n(L, 0) = H(L, L - h_L) \cdots H(h_1, 0). \tag{5}$$

Note that the RK4IP used here is different from the RK4IP in Ref. [14], where what to be solved was the noise-free signal (a 1D matrix), while here what we want is the noise propagator (a 2D matrix). whose computational complexity is $O(N_W^3)$, due to that each \hat{k}_i ($i = 2, 3, 4$) in Eq. (2) needs one general matrix multiplication.

2.2. Equivalent noise propagator of a multi-span system

As discussed in the Appendix, the ASE from an EDFA can be modeled as additive white Gaussian noise (AWGN) with its variance given by Eq. (39). Given the ASE injected at the input of a fiber and the noise propagator obtained from Eqs. (2), (4), and (5), the noise PSD (or PG) at the output of a fiber of length L can be written as [1, 5, 7, 8]

$$PG_1 = p_n(L, 0) \sigma^2 I p_n^T(L, 0) = \sigma^2 p_n(L, 0) p_n^T(L, 0), \tag{6}$$

where I is a unit matrix and Eq. (39) has been used. In Eq. (6), p_n^T is the transpose of p_n .

For a K -span system consisting of $(K + 1)$ EDFAs (cf. Fig. 4), its PG has the form

$$\begin{aligned}
\widehat{PG} &= (G\sigma_{in}^2 + \sigma^2) P_n(K, 0) P_n^T(K, 0) + \sigma^2 \sum_{k=1}^K P_n(K, k) P_n^T(K, k), \\
P_n(K, k) &= p_n(KL, (K-1)L) \cdots p_n((k+1)L, kL), \quad (k = 0, 1, \dots, K-1) \\
P_n(K, K) &= I,
\end{aligned} \tag{7}$$

where $\sigma_{in}^2 = N_{in}/(2T_0)$ and σ^2 is given by Eqs. (28) and (39). In Eq. (7), the real symmetric matrix \widehat{PG} is positive definite. It can be factorized as

$$\widehat{PG} = \sigma^2 P_{n,eq} P_{n,eq}^T, \tag{8}$$

where the equivalent noise propagator $P_{n,eq}$ can be obtained either by using Cholesky decomposition or symmetric (square root) decomposition [16]. The later yields $P_{n,eq} = P_{n,eq}^T$. Our calculation confirms that both decompositions result in the same BER. Note that the $P_{n,eq}$ obtained from Eq. (8) does not necessarily mean it can provide all the noise information. For example, the real unitary matrix associated with a phase shift in noise will lead to the same

PG. This phase shift in noise will not affect the signal-signal beating and noise-noise beating. But it will affect the signal-noise beating. Our numerical results in subsection 5.2 show that a deterministic phase shift in noise will significantly affect the calculated BER. Based on the experimental data, we find that this phase shift is related with the variance of Gordon-Mollenauer phase noise. Here we name it the GM shift Δ_{GM} .

3. BER calculation

With the noise propagator matrix obtained from the accurate LNE, one can evaluate the BER in the OFC system by calculating the moment-generating function (MGF) of the electrically filtered current $I(t_s)$ using Karhunen-Loève series expansion (KLSE).

3.1. Filtered photoelectric current expressed using KLSE

Given a linear optical system, based on the discussions in Ref. [17] and the notations introduced in Ref. [18], the filtered photoelectric current $I(t)$ can be expressed in the form of $I(t) = [\langle s^o(t + T_b) + n^o(t + T_b) | s^o(t) + n^o(t) \rangle + c.c.]/2$. Here $s^o(t)$ ($n^o(t)$) represents the signal (noise) field at the input of the optical filter. Dirac bra $\langle x|$ is the conjugate transpose (or Hermitian transpose) of Dirac ket $|x\rangle$ [$x = s^o(t), n^o(t), s^o(t) + n^o(t), etc.$]. The Dirac ket differs from usual complex vector in that the i th element of the later is just the i th Fourier coefficient of the (signal or noise) field, while the i th element of the former is the product of the i th Fourier coefficient and its base function (cf. Eq. (17) in Ref. [18]). According to Refs. [17, 18], the filtered current in a linear system can be formally expressed as $I(t) = y_{ss} + y_{nn} + y_{ns}$ with $(l = -L_s, \dots, L_s; m = -M_n \dots M_n)$

$$\begin{aligned} y_{ss}(t_s) &= [\langle s^o(t_s + T_b) | R_{ss} | s^o(t_s) \rangle + c.c.]/2 = \langle s^o(t_s) | R_{ss}^D | s^o(t_s) \rangle \\ y_{nn}(t_s) &= [\langle n^o(t_s + T_b) | R_{nn} | n^o(t_s) \rangle + c.c.]/2 = \langle N^o | R_{nn}^D | N^o \rangle = \langle Z | \Lambda | Z \rangle \\ y_{ns}(t_s) &= [\langle n^o(t_s + T_b) | R_{ns} | s^o(t_s) \rangle + \langle n^o(t_s) | R_{ns} | s^o(t_s + T_b) \rangle + c.c.]/2 \\ &= [\langle N_{in} | O_{nn}^\dagger R_{ns}^D | s^o(t_s) \rangle + c.c.] = [\langle Z | b^D(t_s) \rangle + c.c.] \end{aligned} \quad (9)$$

where $\Lambda \equiv U^\dagger O_{nn}^\dagger R_{nn}^D O_{nn} U = \text{diag}\{\lambda_1, \dots, \lambda_{2M_n+1}\}$, $|b^D(t_s)\rangle = U^\dagger O_{nn}^\dagger R_{ns}^D |s^o(t_s)\rangle$, and

$$\begin{aligned} (R_{ss}^D)_{l'l} &= (R_{ss})_{l'l} D_{l'l}^{ss}, \quad (R_{nn}^D)_{m'm} = (R_{nn})_{m'm} D_{m'm}^{nn}, \quad (R_{ns}^D)_{ml} = (R_{ns})_{ml} D_{ml}^{ns} \\ D_{l'l}^{ss} &= \frac{e^{j\frac{2\pi l'l}{N}} + e^{-j\frac{2\pi l'l}{N}}}{2}, \quad D_{m'm}^{nn} = \frac{e^{j\frac{2\pi m'l T_b}{T_0}} + e^{-j\frac{2\pi m'l T_b}{T_0}}}{2}, \quad D_{ml}^{ns} = \frac{e^{j\frac{2\pi m'l T_b}{T_0}} + e^{-j\frac{2\pi m'l T_b}{T_0}}}{2}. \end{aligned} \quad (10)$$

In Eqs. (9)-(10), $|Z\rangle$ represents the decoupled Gaussian random variables with zero mean and real part and imaginary part variance of σ^2 . The effects of the optical and electrical filters in the receiver are represented by matrices with their elements being $(O_{nn})_{mm'} = \delta_{m,m'} H_o(\frac{m}{T_0})$, $(O_{ss})_{ll'} = \delta_{l,l'} H_o(\frac{l}{NT_b})$ and $(R_{ss})_{ll'} = H_r(\frac{l'-l}{NT_b})$, $(R_{nn})_{mm'} = H_r(\frac{m'-m}{T_0})$, $(R_{ns})_{ml} = H_r(\frac{l}{NT_b} - \frac{m}{T_0})$. Due to the optical and electrical filters, signal (noise) components outside $\pm L_s$ ($\pm M_n$) can be neglected. Here [17]

$$L_s = \eta N T_b B_o, \quad M_n = \eta B_o T_0, \quad T_0 = \mu \left(\frac{1}{B_o} + \frac{1}{B_r} \right). \quad (11)$$

For a nonlinear optical system, to get the noise propagator from the accurate LNE (35), one needs to separate complex numbers into their real and imaginary parts. Denoting the Re-Im form of a complex matrix x as $\tilde{x} = \begin{pmatrix} \text{Re}\{x\} & -\text{Im}\{x\} \\ \text{Im}\{x\} & \text{Re}\{x\} \end{pmatrix}$ [where x can be any complex matrix in Eq. (9)] and introducing $|n^o\rangle = P_{n,eq}|a_0\rangle$ with $|a_0\rangle$ being the AWGN from EDFA,

$$|\tilde{s}^o\rangle = \begin{bmatrix} \text{Re}\{|s^o\rangle\} \\ \text{Im}\{|s^o\rangle\} \end{bmatrix}, \quad |\tilde{a}_0\rangle = \begin{bmatrix} \text{Re}\{|a_0\rangle\} \\ \text{Im}\{|a_0\rangle\} \end{bmatrix}, \quad |\tilde{Z}\rangle = \begin{bmatrix} \text{Re}\{|Z\rangle\} \\ \text{Im}\{|Z\rangle\} \end{bmatrix}, \quad (12)$$

it is easy to generalize the noise related currents in Eq. (9) as [1, 5, 7, 8, 17]

$$\begin{aligned} y_{nn}(t_s) &= \langle \tilde{a}_0 | \tilde{U} \tilde{\Lambda} \tilde{U}^T | \tilde{a}_0 \rangle \equiv \langle \tilde{Z} | \tilde{\Lambda} | \tilde{Z} \rangle \quad (\tilde{\Lambda} = \tilde{U}^T P_{n,eq}^T \tilde{O}_{nn}^T \tilde{R}_{nn}^D \tilde{O}_{nn} P_{n,eq} \tilde{U} = \text{diag}\{\tilde{\lambda}_1, \dots, \tilde{\lambda}_{4M_n+2}\}) \\ y_{ns}(t_s) &= \langle \tilde{Z} | \tilde{U}^T P_{n,eq}^T \tilde{O}_{nn}^T \tilde{R}_{ns}^D \tilde{O}_{ss} | \tilde{s}^o(t_s) \rangle = \langle \tilde{Z} | \tilde{B} | \tilde{s}^o(t_s) \rangle \equiv \langle \tilde{Z} | \tilde{b}(t_s) \rangle \quad (\tilde{B} = \tilde{U}^T P_{n,eq}^T \tilde{O}_{nn}^T \tilde{R}_{ns}^D \tilde{O}_{ss}), \end{aligned} \quad (13)$$

where $P_{n,eq}$ can be obtained from Eqs. (2)-(5) and (7)-(8).

3.2. BER obtained from MGF

Averaging $|\tilde{Z}\rangle_i$ ($i = 1, \dots, 4M_n + 2$) using formula [17, 18]

$$E[e^{s(\tilde{\lambda}c^2 + 2c\tilde{b})}] = \int_{-\infty}^{\infty} \frac{dc}{\sqrt{2\pi\sigma^2}} e^{-\frac{c^2}{2\sigma^2}} e^{s(\tilde{\lambda}c^2 + 2c\tilde{b})} = \frac{e^{\frac{2\sigma^2 s^2 \tilde{b}^2}{1-2\sigma^2 s \tilde{\lambda}}}}{\sqrt{1-2\sigma^2 s \tilde{\lambda}}}, \quad (14)$$

the MGF of the filtered current, denoted as $\Psi_{t_s}(s)$ here, can be written as

$$\Psi_{t_s}(s) = E[e^{sI(t_s)}] = e^{sI_{ss}(t_s)} \prod_{i=1}^{4M_n+2} \frac{e^{\frac{2\sigma^2 s^2 \tilde{b}_i^2(t_s)}{1-s\beta_i}}}{(1-s\beta_i)^{\xi}}, \quad (\beta_i = 2\sigma^2 \tilde{\lambda}_i) \quad (15)$$

where $\tilde{b}_i(t_s)$ is the i th component of $|\tilde{b}(t_s)\rangle$ in (13). In this work, we take $\xi = 1/2$ for polarized noise. The BER can be obtained from (15) with [17]

$$\text{BER}_{y_{th}}(t_s) = \frac{\pm 1}{2\pi j} \int_{C_{\pm}} \frac{\Psi_{t_s}(s)}{s} e^{-sy_{th}} ds, \quad (16)$$

where y_{th} is the detection threshold, $+$ and C_+ correspond for $I^{ss} < y_{th}$, while $-$ and C_- for $I^{ss} > y_{th}$. Averaging BERs over all bits in the de Bruijn sequence ($N = 32$ in this work), we have ($t_s = t_0 + sT_b$, $s = 0, \dots, N-1$)

$$\text{BER} = \sum_{s=0}^{N-1} \text{BER}_{y_{th}}(t_s) / N. \quad (17)$$

4. OSNR at the receiver

For an optical system with ASE power being much larger than other noise sources, the OSNR with reference bandwidth B_r (0.1nm) can be calculated as

$$\text{OSNR}_{0.1nm} = \frac{\bar{P}_s}{P_{ASE}(B_r)}. \quad (18)$$

In Eq. (18), \bar{P}_s is the time-averaged (noise free) signal power, while $P_{ASE}(B_r)$ is the noise power within B_r . To obtain \bar{P}_s and $P_{ASE}(B_r)$, one needs to notice that the measurement bandwidth B_m [e.g., the bandwidth of the transfer function of an optical spectrum analyzer (OSA)] may not be the same as B_r . Thus the \bar{P}_s in Eq. (18) becomes the power of the signal filtered by B_m , while $P_{ASE}(B_r)$ becomes the ASE filtered by B_m and weighted by a factor B_r/B_m [19].

In a linear optical system, the ASE noise along the fiber can be treated as AWGN (additive white Gaussian noise). Thus, for the system of Fig. 4, its OSNR can be simply calculated as

$$\text{OSNR}_{L,0.1nm} = \frac{\bar{P}_s}{P_{ASE}(B_m)} \times \frac{B_m}{B_r} \quad \left(P_{ASE}(B_m) = [GN_{in} + N_0(K+1)]B_m \right), \quad (19)$$

where $P_{ASE}(B_m)$ is the ASE power within B_m and N_0 is given by Eq. (28). In Eq.(19), the filter (B_m) effect on the ASE has been neglected.

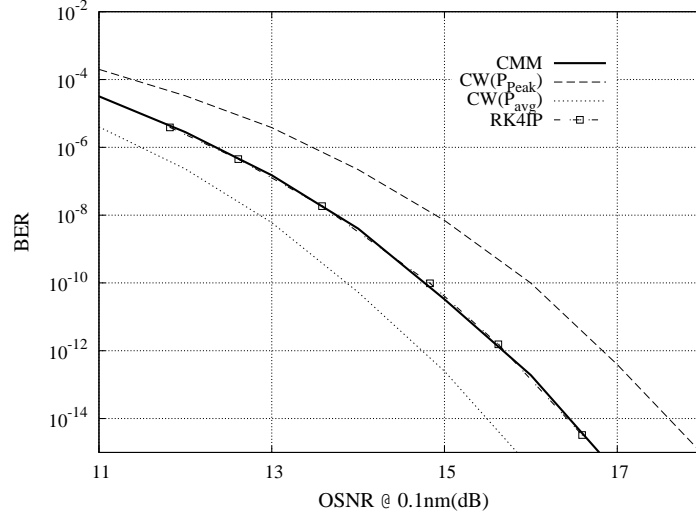


Fig. 1. BER versus received OSNR for a 20Gb/s 20-span RZ-DPSK system with $\Phi_N = 0.2\pi$. Solid: obtained using CMM of Ref. [1]. Dashed (dotted): improved CW approach of Ref. [5] with CW power being peak power (average power), respectively. Dash-dotted: RK4IP approach. All curves, except the dash-dotted, are obtained from Fig. 8 of Ref. [5].

In a nonlinear optical system, the ASE noise “amplified by” PG cannot be treated as a white noise. Similar to the noise-noise beating given in Eq. (13), the measured ASE power will only relate with the self-beating terms of the noise, which yields

$$OSNR_{NL,0.1nm} = \frac{\bar{P}_s}{P_{ASE}(B_m)} \times \frac{B_m}{B_r} \left(P_{ASE}(B_m) = Tr(O_m^T \widehat{PG} O_m) \sigma^2 = Tr(\widehat{PG} O_m O_m^T) \sigma^2 \right). \quad (20)$$

Here O_m is the low-pass transfer function of the bandpass filter (bandwidth B_m). In Eq. (20), σ^2 and \widehat{PG} are given by Eq. (39) and Eq. (7), respectively.

In the case of traditional OSA-based out-of-band OSNR monitoring, the ASE power can be interpolated using

$$P_{ASE}(B_m, \pm\Delta\lambda) = \frac{Tr\left[\widehat{PG}\left(O_m(-\Delta\lambda)O_m^T(-\Delta\lambda) + O_m(+\Delta\lambda)O_m^T(+\Delta\lambda)\right)\right]\sigma^2}{2}, \quad (21)$$

where $O_m(\pm\Delta\lambda)$ is the filter function centered at $\pm\Delta\lambda$. When $\Delta\lambda = 0$, Eq. (21) returns to the ASE power in Eq. (20), where $P_{ASE}(B_m) \equiv P_{ASE}(B_m, 0)$.

5. Applications to DPSK systems

To show that the new approach to get the noise propagator is numerically applicable, we will compare our RK4IP results with the CMM results given by Ref. [5] and with the experimental data given by Ref. [7]. Both consider systems with $R_b = 20\text{Gb/s}$, using RZ-50% DPSK modulation. In the receiver, the optical filter is Gaussian type, while the electric filter is the fifth-order Bessel type. In the following calculations, we set $T_0 = NT_b$ by changing μ in Eq. (11).

5.1. Comparison with CMM results

We consider the 20-span DPSK system discussed in Ref. [5], where BERs using the CMM and the (improved) CW approaches were plotted against the received OSNR in the Fig. 8 of

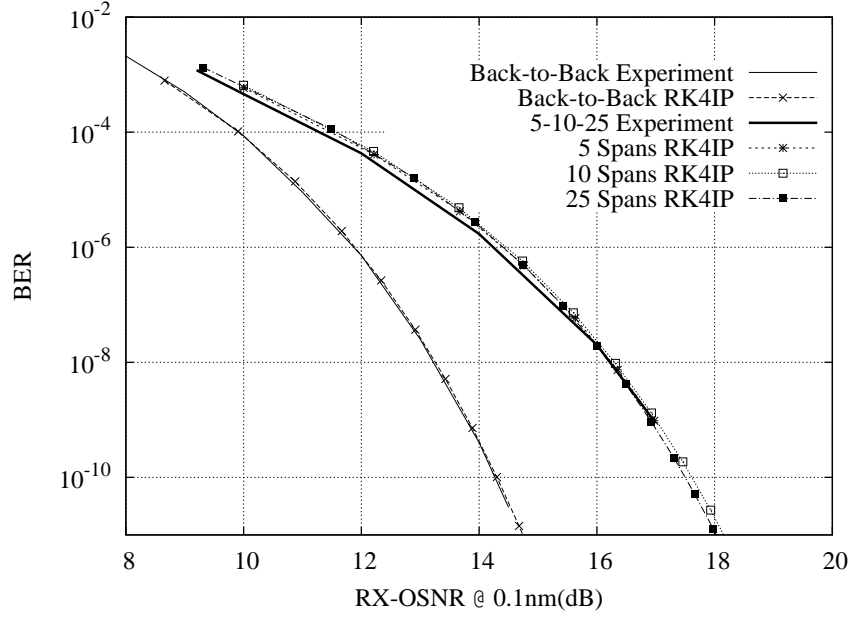


Fig. 2. BER versus received OSNR for the multi-span RZ-50% DPSK systems with $\bar{\Phi}_N = 0.9$. According to Fig. 7 (b) in Ref. [7], where the experimental curves for 5-, 10-, and 25-span systems were almost the same, here we replot them using a thick solid curve.

Ref. [5]. In fact this system is basically the same as the one shown in Fig. 4 in the Appendix, provided that one removes the pre- and postcompensating fibers and their amplifiers in the Fig. 2 of Ref. [5] and removes the first EDFA and N_{in} in our Fig. 4. Thus the first term of \widehat{PG} [in Eq. (7)] needs to be ignored. Like [5, 20], where OSNR was calculated in the absence of PG, we obtain OSNR from Eq. (19) with $N_{in} = 0$ and $(K + 1)$ being replaced by K . According to Ref. [5], we change OSNR by changing the n_{sp} in Eq. (28). As plotted in Fig. 4, each span contains a transmission fiber followed by a dispersion-compensating fiber (DCF). The transmission fiber is $l = 100$ km long with its CD parameter $D_{tx} = 8$ ps/nm/km. Each span is fully compensated. The nonlinear phase accumulated in the fiber, generally defined as $\bar{\Phi}_N = \int \gamma \bar{P}(z) dz$ with $\bar{P}(z)$ being the time averaged signal power, is 0.2π . The bandwidth of the optical (electrical) filter in the receiver is $B_o = 1.8R_b$ ($B_e = 0.65R_b$), respectively.

To let our results be reproducible, we provide, as detailed as possible, other related parameters below. The DCF in each span is 8 km long with $D_{DCF} = -100$ ps/nm/km. Transmission fiber and DCF are assumed to have same fiber loss ($\alpha = 0.2$ dB/km) and same nonlinear coefficient ($\gamma = 2.0$ /W/km). The EDFA in each span is used to compensate the total loss in the fiber of $L = (100 + 8)$ km. Therefore the signal power at the input of each span, P_{in} , keeps constant. Ignoring the nonlinear phase contribution of DCF [21], we set $P_{in} = 0.7307$ mW, obtained from $\bar{\Phi}_N = K\gamma P_{in}(1 - e^{-\alpha l})/\alpha = 0.2\pi$ with $K = 20$ and $l = 100$ km. The OSNR is obtained using Eq. (19) with $B_m/B_r = 1.35$.

As shown in Fig. 1, the curve using the proposed RK4IP approach (dash-dotted) agrees very well with the CMM curve (solid) given by Ref. [5]. In Fig. 1, the curves using improved CW approach [5] with CW power being transmitted peak power (dashed) and average power (dotted) are plotted for comparison.

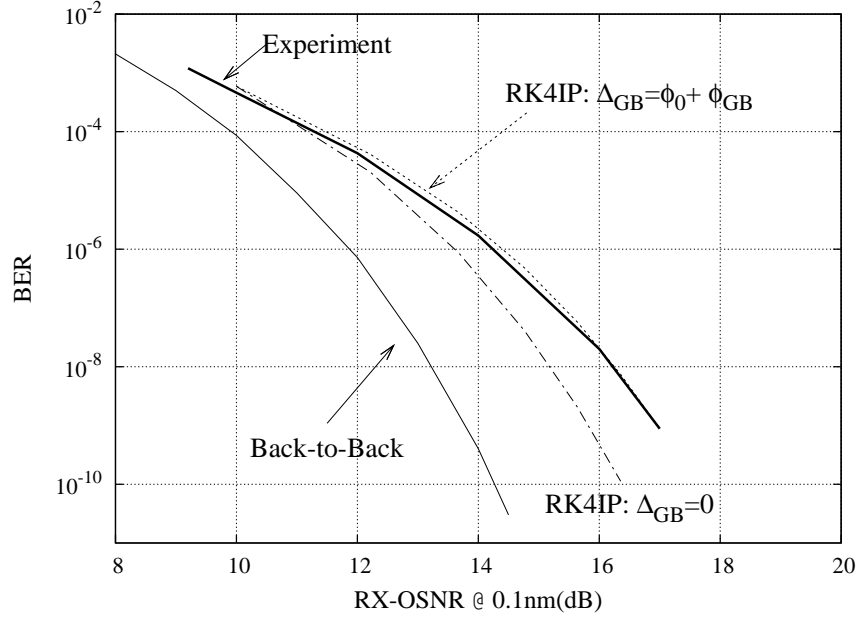


Fig. 3. BER vs RX-OSNR for the 5-span RZ-50% DPSK system with $\bar{\Phi}_N = 0.9$. Solid: experimental results. Dotted (Dash-dotted): numerical calculation using RK4IP with (without) GB shift.

5.2. Comparison with experimental data

The optical system discussed in Ref. [7] can be modelled by Fig. 4, except that each EDFA should be replaced by an EDFA followed by an optical filter (Gaussian) O_{lk} with bandwidth of 5 nm. Also, the input noise N_{in} needs to be filtered by an optical filter O_{in} (Gaussian, 5 nm). As a result, in Eq. (7), the noise propagator $p_n((k+1)L, kL)$ ($k = 0, \dots, K-1$) should be replaced with $O_{lk}p_n((k+1)L, kL)$, $P_n(K, K) = 1$ with $P_n(K, K) = O_{lk}$, and $G\sigma_{in}^2 P_n(K, 0)P_n^T(K, 0)$ with $G\sigma_{in}^2 P_n(K, 0)O_{in}O_{in}^T P_n^T(K, 0)$. Since we only consider the BER vs RX-OSNR curves for the multi-span systems plotted in Fig. 7 (b) of Ref. [7], each fiber (L km long) in Fig. 4 contains a SMF followed by a DCF. In our calculation, all the related fiber parameters are same as those given in Table 1 of Ref. [7]. In the receiver, the bandwidth of the optical filter is $1.87R_b$, while the bandwidth of the electrical filter is $0.75R_b$.

We first consider the back-to-back case. Similar to Ref. [7], we modify the 20Gb/s RZ-50% signal at the transmitter by comparing its calculated spectrum [22] and its measured spectrum[7]. Due to that the input noise N_{in} is filtered by O_{in} , the OSNR is calculated using Eq. (20) with $B_m/B_r = 0.95$, yielding the back-to-back RK4IP curve shown in Fig. 2.

For the 5-, 10-, 25-span systems, their accumulated nonlinear phases are calculated according to Eq. (48) of Ref. ([7]). Because of the spectral modification of the input signal, the optical power at the input of each span $P_{in} = P_{SMF}$ is smaller than E_b/T_b , where E_b is the energy per bit before the spectral modification. For example, to get nonlinear phase $\bar{\Phi}_N = 0.9$ for the 25-span system, the fiber input power $P_{in} = P_{SMF}$ should be 1.516 mW, which means $E_b/T_b = 0.127$ mW or $GE_b/T_b = 2.316$ mW ($G = 18.197$). Different from the DPSK receiver shown in Fig.4, where the delay is $T_b = 1/R_b = 50$ ps, the delay in the receiver of Ref. [7] was $T'_b = 24.84$

GHz)⁻¹=40.26 ps. Thus, the DPSK phase factors given in Eq. (10) should be modified as

$$D_{l'l}^{ss} = \frac{e^{j\frac{2\pi l'}{N'}} + e^{-j\frac{2\pi l'}{N'}}}{2}, \quad D_{m'm}^{nm} = \frac{e^{j\frac{2\pi m' T'_b}{T_0}} + e^{-j\frac{2\pi m' T'_b}{T_0}}}{2}, \quad D_{ml}^{ns} = \frac{e^{j\frac{2\pi m' T'_b}{T_0} - j\Delta_{GM}} + e^{-j\frac{2\pi l'}{N'} + j\Delta_{GM}}}{2}, \quad (22)$$

with $N' = N(T_b/T'_b)$, $T'_b = T_b + \Delta T_b$. In Eq. (22), the phase shift discussed after Eq. (8) is introduced as

$$\Delta_{GM} = \phi_0 + \phi_{GM} \equiv \phi_0 + \arctan(\sqrt{OSNR}). \quad (23)$$

To get all the RK4IP curves plotted in Fig. 3, we set $\phi_0 = -\arctan(\sqrt{10}) = -1.26$, whereas the ASE power is calculated using Eq. (21) with $\Delta\lambda = 2B_m$. Here, ϕ_0 is a calibration constant that basically shifts the RK4IP curves in the OSNR direction, while $\arctan(\sqrt{OSNR})$ determines the slope of the RK4IP curves. To show this, we plot in Fig. 3 the RK4IP results for the 25-span system with $\Delta_{GM} = -1.26 + \arctan(\sqrt{OSNR})$ and $\Delta_{GM} = 0$. Also, we consider the RK4IP curves using Eq. (20) to calculate ASE power. Our results for the 5-span, 10-span, and 25-span systems confirm that there is almost no difference between the the curve using Eq. (21) with $\phi_0 = -1.26$ and the curve using Eq. (20) with $\phi_0 = -1.00$. How to evaluate ϕ_0 for a given OSNR monitoring technique is expected to be studied elsewhere.

6. Summary

For an OFC system with low BER, e.g., $< 10^{-9}$, efficient way to evaluate the BER is to calculate the MGF of the filtered photoelectric current using KLSE. Within linear perturbation, the noise impact on MGF (and BER) can be obtained by calculating the noise propagator.

Different from the CMM approaches in Refs. [1, 10, 11], a new approach is proposed here to get the noise propagator from the accurate LNE using RK4IP method. This approach does not need the jitter separation required by CMM. To numerically verify this new approach, we consider a 20-span RZ-DPSK system discussed in Ref. [5]. The BERs obtained using this new RK4IP agree well with those using CMM in Ref. [5].

As discussed after Eq. (8), conventional noise propagator obtained by factoring the PG has an uncertainty caused by a phase shift in noise. By comparing our results with the experimental data of Ref. [7], we find that this deterministic shift is related with the Gordon-Mollenauer phase noise variance and it will affect the BER significantly. Further study on such phase shift is expected to provide a new approach to reduce the impact of the noise-signal interaction on OFC systems.

Appendix: Accurate LNE in the EDFA-based systems

The optical field $u(z, t)$ in a fiber satisfies

$$\frac{\partial u}{\partial z} = j\frac{\beta_{\omega\omega}}{2}\frac{\partial^2 u}{\partial t^2} + \frac{\beta_{\omega\omega\omega}}{6}\frac{\partial^3 u}{\partial t^3} - j\gamma|u|^2u - \frac{\alpha}{2}u, \quad (24)$$

where α is the fiber loss and $\beta_{\omega\omega} = \partial^2\beta/\partial\omega^2$ relates to the CD parameter $D(\lambda)$ (ps/nm/km) with $\beta_{\omega\omega} = -\frac{\lambda^2 D(\lambda)}{2\pi c}$ ($c=3\times 10^8$ m/s). The slope parameter $\beta_{\omega\omega\omega} = (\frac{\lambda}{2\pi c})^2 [2\lambda D(\lambda) + \lambda^2 D'(\lambda)]$ [$D'(\lambda) = \frac{dD(\lambda)}{d\lambda}$ (ps/nm²·km)] can be neglected if bit rate R_b satisfies $R_b > |\beta_{\omega\omega}/\beta_{\omega\omega\omega}|$ [17].

Introducing the transformation $u(z, t) = v(z, t)e^{-\alpha z/2}$, Eq. (24) can be reduced as

$$\frac{\partial v}{\partial z} = j\frac{\beta_{\omega\omega}}{2}\frac{\partial^2 v}{\partial t^2} + \frac{\beta_{\omega\omega\omega}}{6}\frac{\partial^3 v}{\partial t^3} - je^{-\alpha z}\gamma|v|^2v. \quad (25)$$

In a K -span system amplified by $(K+1)$ EDFAs (cf. Fig. 4), Eq. (25) can be modified as

$$\frac{\partial v}{\partial z} = j\frac{\beta_{\omega\omega}}{2}\frac{\partial^2 v}{\partial t^2} + \frac{\beta_{\omega\omega\omega}}{6}\frac{\partial^3 v}{\partial t^3} - je^{-\alpha z}\gamma|v|^2v - jw(z, t), \quad (26)$$

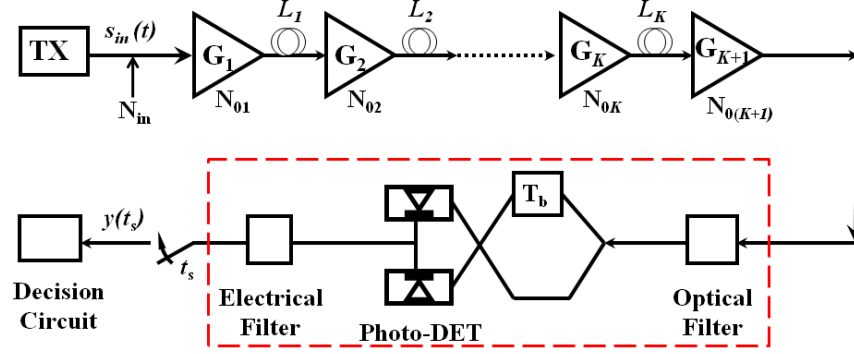


Fig. 4. Low-pass equivalent optical model. The receiver consists of optical and electrical filters and DPSK balance detection. Discussions here (except those detailed in Sec. 5) are based on the assumptions that $N_{0k} = N_0$ and $G_k = G$ [$k = 1, 2, \dots, (K+1)$]. Also, the fiber in each span is assumed to have same length (L km) and same loss (α dB/km).

where $w(z, t)$ is the ASE forcing modeled as the complex AWGN with correlation

$$r(z, z', t, t') = E\{w(z, t)w^*(z', t')\} = \delta(t - t')\delta(z - z') \sum_{k=1}^{K+1} N_{0k} \delta(z - (k-1)L). \quad (27)$$

In Eq. (27), the fiber length in each span is assumed to be L (km) long, According to Wiener-Kinchine theorem [23], N_{0k} in Eq. (27) is the ASE PSD (in one polarization direction) at the output of the k th EDFA. Suppose each EDFA has the same gain G and spontaneous-emission parameter n_{sp} , we have [17]

$$N_{0k} = N_0 = n_{sp}(G-1)\hbar\omega \quad (k = 1, 2, \dots, K, (K+1)) \quad (28)$$

Decomposing optical field $v(z, t)$ in the fiber into noise-free field $v_0(z, t)$ and its perturbation $\delta v(z, t)$ [i.e., $v(z, t) = v_0(z, t) + \delta v(z, t)$] and assuming that $|v_0| \gg |\delta v|$ (so that the nonlinear terms of δv can be neglected), Eq. (26) can be decomposed as [1]

$$\frac{\partial v_0}{\partial z} = j\frac{\beta_{\omega\omega}}{2} \frac{\partial^2 v_0}{\partial t^2} + \frac{\beta_{\omega\omega\omega}}{6} \frac{\partial^3 v_0}{\partial t^3} - je^{-\alpha z} \gamma |v_0|^2 v_0 \quad (29)$$

$$\frac{\partial \delta v}{\partial z} = j\frac{\beta_{\omega\omega}}{2} \frac{\partial^2 \delta v}{\partial t^2} + \frac{\beta_{\omega\omega\omega}}{6} \frac{\partial^3 \delta v}{\partial t^3} - j2e^{-\alpha z} \gamma |v_0|^2 \delta v - je^{-\alpha z} \gamma v_0^2 \delta v^* - jw(z, t). \quad (30)$$

Noise equation Eq. (30) differs from common equations in that the real and imaginary parts of the complex noise field need to be treated separately [1].

Denoting $a_l = a(\omega_l) = \int \delta v e^{-j\omega_l t} dt$ and $[M_v]_{lm} = v_{l-m}$, $[M_\mu]_{lm} = \mu_{l+m}$ with

$$v_l = v(\omega_l) = e^{-\alpha z} \int |v_0|^2 e^{-j\omega_l t} dt, \quad \mu_l = \mu(\omega_l) = e^{-\alpha z} \int v_0^2 e^{-j\omega_l t} dt, \quad (31)$$

in frequency domain, Eq. (30) has the form

$$\frac{da_l}{dz} = -j\frac{\beta_{\omega\omega}}{2} \omega_l^2 a_l - j\frac{\beta_{\omega\omega\omega}}{6} \omega_l^3 a_l - j2\gamma(z)[M_v]_{lm} a_m - j\gamma(z)[M_\mu]_{lm} a_m^* - jW_l, \quad (32)$$

where $W_l = W(z, \omega_l)$ is the Fourier component of the forcing term $w(z, t)$ in Eq. (26). As indicated in Ref. [1], since $|v_0|^2$ in (31) is real, $v_l = v_{-l}^*$. So M_v in (32) is Hermitian, or, its real part M_v^R is symmetric, while its imaginary part M_v^I is anti-symmetric. Also, as $[M_\mu]_{km} = \mu_{k+m}$, both the real (M_μ^R) and imaginary parts (M_μ^I) of M_μ are symmetric.

The matrix form of Eq. (32) is

$$\frac{da}{dz} = \bar{L}a + va + \mu a^* - jW \quad (33)$$

$$\bar{L} = jL_{CD}, \quad v = -2j\gamma(z)(M_v^R + jM_v^I), \quad \mu = -j\gamma(z)(M_\mu^R + jM_\mu^I) \quad (34)$$

Introducing $\tilde{a} = (a_R, a_I)^T$ (for $a = a_R + ja_I$) and $\tilde{W} = (W_I, -W_R)^T$ (for $-jW = W_I - jW_R$), Eq. (33) is equivalent to

$$\frac{d\tilde{a}}{dz} = (\hat{L} + \hat{v} + \hat{\mu})\tilde{a} + \tilde{W} \quad (35)$$

$$\hat{L} = \begin{pmatrix} 0 & -L_{CD} \\ L_{CD} & 0 \end{pmatrix}, \quad \hat{v} = \begin{pmatrix} v_{AA} & -v_{SS} \\ v_{SS} & v_{AA} \end{pmatrix}, \quad \hat{\mu} = \begin{pmatrix} \mu_R & \mu_I \\ \mu_I & -\mu_R \end{pmatrix}, \quad (36)$$

with $(L_{CD})_{ij} = -[\frac{\beta_{\omega\omega}}{2}\omega^2 + \frac{\beta_{\omega\omega\omega}}{6}\omega^3]\delta_{ij}$, $v_{AA} = 2\gamma M_v^I$, $v_{SS} = -2\gamma M_v^R$, $\mu_R = \gamma M_\mu^I$, and $\mu_I = -\gamma M_\mu^R$. According to the discussion given below Eq. (32), \hat{v} ($\hat{\mu}$) in Eq. (36) is antisymmetric (symmetric), respectively. Calculation of the Kerr term $(\hat{v} + \hat{\mu})$ according to Eq. (36) has the computational complexity much less than $O(N_W^3)$, where N_W is the number of Fourier components used for signal representation. In fact, the computational cost of this way is basically determined by the FFTs in Eq. (31), which has the computational complexity of $O(N_W \log N_W)$.

In frequency domain, ASE correlation relation (27) has its matrix form ($\tilde{W}(\omega_l) \rightarrow \tilde{W}_l \sqrt{\Delta f}$)

$$E\{\tilde{W}_l(z)\tilde{W}_{l'}^*(z')\} = \delta_{z,z'}\delta_{l,l'} \sum_{k=0}^K \frac{N_0}{2T_0} \delta_{z,kL} \quad (l = 1, \dots, 4M_n + 2), \quad (37)$$

where Eq. (28) has been used. In Eq. (37), $T_0 = 1/\Delta f$ and M_n are given by Eq. (11). Eq. (37) means that Eq. (35) can be equivalently replaced by

$$\frac{d\tilde{a}}{dz} = (\hat{L} + \hat{N})\tilde{a}; \quad (\hat{N} = \hat{v} + \hat{\mu}) \quad (38)$$

with boundary condition [24]

$$E\{\tilde{W}(z_f)\tilde{W}^*(z_f)\} = \frac{N_0}{2T_0}I \equiv \sigma^2 I \quad (39)$$

with I being a $(4M_n + 2) \times (4M_n + 2)$ unit matrix and σ^2 being the variance of the real or imaginary part of input ASE.

Acknowledgment

The authors acknowledge the financial support from Canada Research Chair program. The first author sincerely thanks Paolo Serena, Leonardo D. Coelho, and Marco Secondini for providing their detailed calculation information in Refs. [5, 7, 8].